THE EUROPEAN
PHYSICAL JOURNAL PLUS

Regular Article

A low-cost radiation detection system to monitor radioactive environments by unmanned vehicles

Andrea Chierici[1,3,a] , **Andrea Malizia**[1,4]**, Daniele di Giovanni**[1,5]**,**
Francesca Fumian[1,2]**, Luca Martellucci**[1]**, Pasquale Gaudio**[1]**, Francesco d'Errico**[3,6]

[1] Department of Industrial Engineering, University of Rome Tor Vergata, 00133 Roma, Italy
[2] Joint NBC Defence School of Rieti, 02100 Rieti, Italy
[3] Department of Industrial and Civil Engineering, University of Pisa, 56122 Pisa, Italy
[4] Department of Biomedicine and Prevention, University of Rome Tor Vergata, 00133 Roma, Italy
[5] Unicamillus-Saint Camillus International University of Health Sciences, 00131 Roma, Italy
[6] Yale Center for Emergency Preparedness and Disaster Response, New Haven, CT, USA

Abstract Unconventional scenarios with hazardous radioactive levels are expected as consequences of accidents in the industrial sector of the nuclear energy production or following intentional releases of radioactive materials for terrorist purposes (dirty bombs, indoor contaminations, etc.). Nowadays, the need to balance the high standards of safety and security through an effective detection network is a matter of paramount importance. In this work, the authors' challenge has been to design, realize and test a low-cost gamma detection and spectroscopy system which may be used in unmanned vehicles in general and/or drones with low payload capabilities. The designed platform may be used to carry out mapping or localization operations in order to reduce the risk factor for first responders or for the population affected by radiological and nuclear events. In this paper, the design process of a gamma ray detection and spectroscopy system based on affordable and commercially available technologies is presented along with the results of our ongoing characterization of the prototype.

1 Introduction

Unmanned vehicles (UVs) for radiation monitoring have been often utilized in the past decade, and some major technological improvements have been introduced after the incident at the Fukushima Daiichi Nuclear Power Plant (FDNPP) in March 2011 [1–3]. Long-range monitoring, mid-range monitoring, and short-range monitoring were necessary to identify the contaminated areas after the accident. In a radiological and nuclear (RN) event, accurate monitoring of the contamination may be a useful tool to assess the risk for first responders or for the population who may become exposed to an unacceptable amount of radiation.

The field of radiation monitoring can be separated in two distinct categories: localization and mapping [4]. Localization concerns the identification of an individual radioactive source,

---

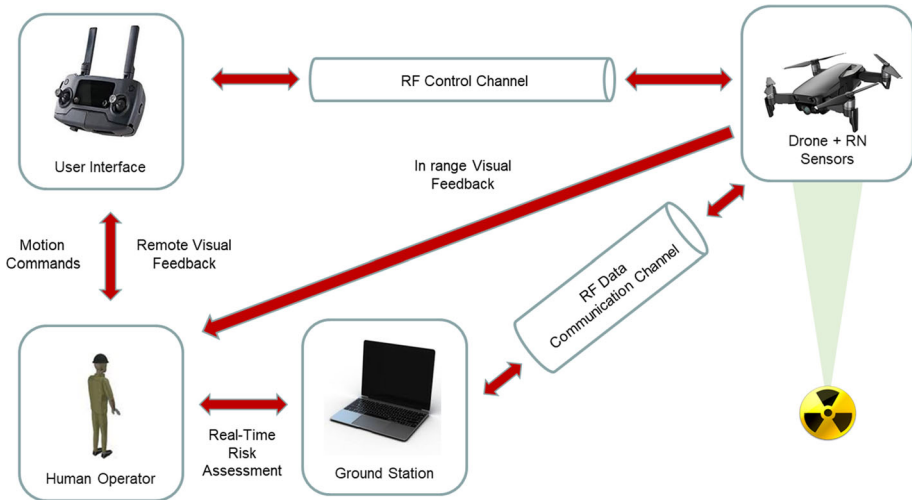[a] e-mail: a.chierici@studenti.unipi.it (corresponding author)

Fig. 1 Aim and final application of the activity

while mapping refers to the task of identifying the distribution of radiation over a given area. Localization and mapping can be both used to quantify areas of risk in order to aid competent authorities in taking countermeasures to protect a workforce or citizens following an event or a disaster.

In terms of unmanned aerial vehicles (UAV), there are several different technologies available, but they fall essentially in just two categories: fixed wing systems, which can reach very high speeds, but suffer from low spatial resolution when conducting radiation surveys, and single or multi rotor systems, which can hover slowly on in a stationary position. The latter are well-suited to conduct radiation monitoring tasks in relatively small areas and over short distances [3–5].

In this work, the feasibility and development stages of an affordable, compact, battery-powered RN detection system are described; the system has been specifically designed and realized to be mounted on an UAV, a multi-copter of mini category (Maximum Take-Off Weight (MTOW) less than 25 kg) that can operate to detect and map contamination before the intervention of first responders and thus reduce the risk factor for the exposed operators.

The schematic diagram of this project is reported in Fig. 1.

A real-time analysis is performed in a ground station to evaluate the risk factor related to the mapped area. Data communication must be independent from the channel used to remotely control the drone and must be performed in accord to AEP-84, covered by STANAG 4586 [6], ADatP-36, covered by STANAG 5527 [7] and APP-11, STANAG 7149 [8].

In terms of detection capabilities, since charged particles (such as betas and alphas) are characterized by relatively short-ranges in air, the main focus of the work has been on measuring gamma rays.

1.1 Overview

Among the available RN detection technologies, scintillation detectors offer a relatively high detection efficiency in a small active volume, while potentially keeping the development costs low. In scintillation spectroscopy, the energy spectrum of a gamma ray field is mea-

sured by converting the gamma rays into visible light pulses inside the scintillator material. The light pulses are then sensed by a low-level light detector attached to the scintillator. Common choices for the light detector include photomultiplier tubes (PMT), PIN photodiodes, avalanche photodiodes (APD), or more recently, silicon photomultipliers (SiPM) [9–11].

The light emission in the scintillator decays over a time scale that is characteristic of the particular material employed, ranging from fractions of ns to several µs. Commonly, the light pulse is converted into an electrical signal, and a charge sensitive preamplifier (CSP) is used to integrate the resulting current pulse from such light detector into a voltage pulse. The CSP voltage pulse height is proportional to the total charge release by the photoelectron. In such configuration, the output voltage of the CSP, namely the pulse height, provides a measure of the ionization energy deposited in the scintillator by the gamma ray.

Different approaches can be used to measure and process the CSP output voltage. In analog signal processing, the signal-to-noise ratio of the acquisition chain is improved by the application of a gaussian shaping amplifier (SA) to the CSP signal before the pulse height is measured. The SA has the functionality of a bandwidth filter and of a signal amplifier. Moreover, thanks to the high-pass component of the filter, the long tail from the CSP output is removed allowing to mitigate the pulse-pileup between nearby events in time.

In order to collect and digitize such signals, the conversion technique of choice always involves a trade-off between the available hardware resources, costs, space and power consumption.

In digital signal processing (DSP) methods, the output of the CSP is recorded using a high-speed analog-to-digital converters (ADC) with sampling rates on the order of 500,000 samples per second (Sps) or more. A common method employed in DSP involves the convolution of the measured CSP signal with a trapezoidal filter; such filter has a rise time which has the same functionality of the shaping time of an analog SA [10]. In another digital approaches, the light detector's output is digitized directly at even higher rates (> 250 MSps). High-rate digitization is used when temporal pulse shape information is desirable such as in pulse shape discrimination [12].

Development boards based on commercially available microcontrollers (such as the widely used Atmel Atmega328p or the newer Atmel Atmega4809) have an ADC sampling rate which is in the order of 50 kSps [13, 14]. Such relatively slow sampling time compared to the light pulse width means the analog pulse height cannot be directly measured accurately. The solution in this case is to employ a peak detector (PKD), a well-established analog circuit that allows the conversion of transient voltage pulse heights into persistent voltages [9]. Another approach is to employ time over threshold (TOT) techniques, where timers are used to record the width of the pulses which are then associated with the pulse height [15–17]. The two techniques share some common core components, such as a preamplifier-shaper-discriminator chain.

In this work, a compact and affordable gamma ray detection and spectroscopy system was designed, realized and tested. The system is based on a commercial analog front-end (AFE) consisting in a CSP and a SA interfaced with an Atmega4809 microcontroller; the microcontroller was accessed and programmed through an Arduino Nano Every development board. The Atmega4809, together with some extra components and integrated circuits, was configured to fulfil the role of a multi-channel analyzer (MCA) using both PKD and TOT conversion techniques. In order to grant mid- and long-range communication capabilities to the setup, an inexpensive radio frequency trans-receiver communication module was also installed on the platform. Since the system is battery powered, lightweight, compact and affordable, it is suitable to be mounted on an UAV for short- to mid-range radiation monitoring tasks.
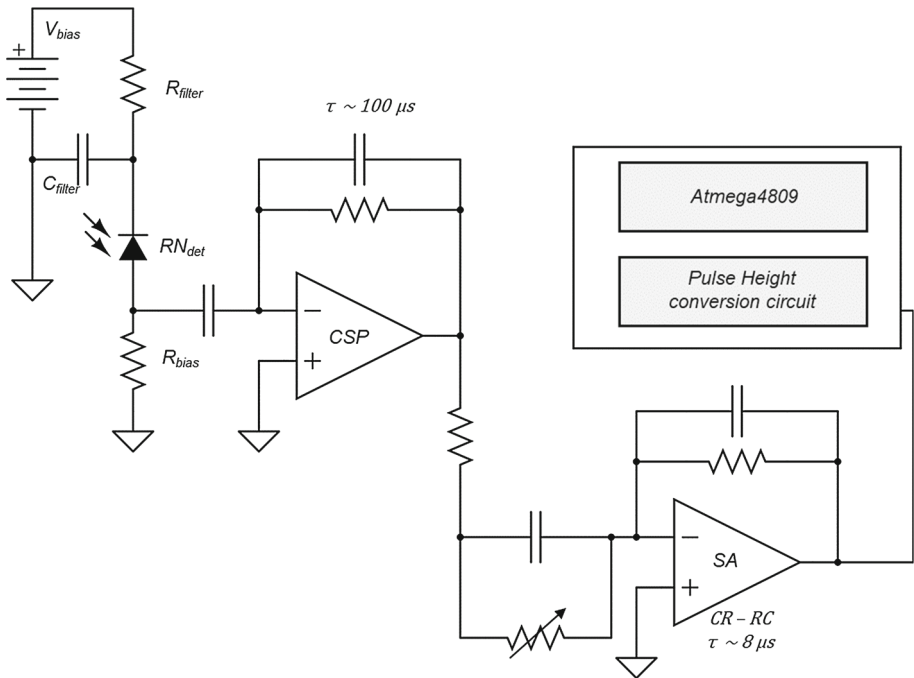
Fig. 2 Electronic architecture of the gamma radiation readout system

This paper is organized as follows. The working principles and the basic components required for the PDK and TOT conversion techniques are reviewed first, then the individual components of the specific systems and some of the underlying physics are presented. The realization of the prototypes is then described together with the results of a charge calibration. Finally, examples of recorded gamma ray spectra and the next experiments to be conducted are presented together with the required steps to completely automatize the radiation monitoring tasks.

2 System components

The general features of our circuit are shown in Fig. 2. The detector is biased using a positive step-up voltage power supply and coupled to the AFE consisting of a CSP and a SA. The output of the SA is fed to a circuitry based on an Atmega4809 microcontroller which has been specifically designed to perform a PKD or TOT conversion of the input signals. A brief description of each component follows, beginning with the scintillation detector and working through the acquisition signal chain.

2.1 Scintillation detector and analog front-end

We employed a CsI(Tl) crystal as a scintillation detector acquired from Micod and AlexDe-tector companies with dimensions of 10 mm × 10 mm × 40 mm and wrapped with a Teflon -based reflector tape. The scintillator is coupled to a PIN diode having an active area of 25 mm^2. CsI(Tl) was chosen because it has a high light yield of 40–60 photons per keV of
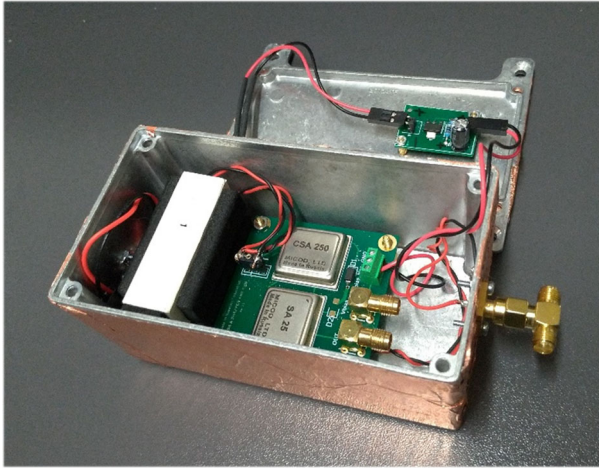
Fig. 3 Scintillation detector and analog front-end assembly

deposited energy and adequate energy resolution. The emission wavelength peaks at around 550 nm, and the signals generated from the PIN diode are sufficiently large to be measured. CsI(Tl) is also less hygroscopic than other scintillators such as NaI(Tl), so that it can be handled without the need for hermetic encapsulation [9, 18].

The AFE consists of a low-cost hybrid circuit preamplifier module (Micod CSA 250) and of a dedicated SA module (Micod SA 25) mounted on a two-layer evaluation board. Current consumption for the whole board is in the order of few mA. The specified pulse height sensitivity of the CSP is 10 V per pC, and it features a decay time of 100 μs. Such sensitivity has been considered appropriate when using a PIN diode coupled with the scintillation crystal since no internal electronic amplification process is present; however, if a different optical sensing element is used—such as a SiPM—then a CSP featuring a lower gain should be chosen as well. The choice of a lower gain CSP may also improve the noise levels of the AFE in terms of pure electronic noise and electro-magnetic interference noise (EMI) pick-up.

The SA is a CR–RC gaussian shaping amplifier, with a shaping time roughly equal to 8 μs (total pulse width roughly equal to 25 μs). SA(s) are required to improve the signal-to-noise ratio of the analog signal acquisition chain in presence of an high gain CSP (such as in this case), and they act as both a bandwidth filter and a signal amplifier; they also remove the long tail from the preamplifier output to alleviate pulse-pileup between nearby events in time. No baseline restoration circuitry was implemented, so the behaviour of the readout may result degraded in the presence of very high counting rates. However, since the scintillator is relatively small, the event rate is also low. The assembly of the detector and of the AFE is shown in Fig. 3.

Nevertheless, if the counting rate is on the order of the pulse processing time (roughly 100–200 μs), a distortion of the measured spectrum is possible. We have not yet developed a dead time model for this system, but it would be influenced by the readout processing time and by managing the communication between the microcontroller and any other devices such as a serial interface or a radio transmitting device.

Based on a market survey conducted prior to the development of the system, some alternative AFE(s) were identified as potential candidates to substitute the current one, such as Cremat CR11x charge amplifiers, CR200 shaping amplifiers, and CR210 baseline restorers.

While more expensive, they offer the potential to fully customize the sensitivity and shaping time of the AFE; moreover, the baseline restorer module allows to alleviate the distortion of the spectra when a very high counting rate is present. Another potential candidate to carry out the detection task are Scionix scintillation detectors equipped with a SiPM readout, which promise a lower level of electronic noise compared to PIN diode-based solutions at expense of an increased electronic complexity. Since the system presented in this paper is completely modular, different types of detectors and AFE(s) may be tested in the future to find the optimum balance between performance and costs.

2.2 Atmega4809 microcontroller

There are several requirements on the microcontroller chosen for the data acquisition tasks and on the other supporting components. Specifically, timing constraints and response predictability are mandatory when developing a data acquisition system. The ATmega4808/4809 microcontrollers [14] are part of the megaAVR 0-series from Atmel, which uses an AVR processor running up to 20 MHz. Since they offer up to 6 kB of SRAM, a 1024 or 2048 channels spectrum (with each channel, for example, storing up to 2 B of data) can be temporarily stored before being sent to a higher level processing unit (such as a generic laptop, another microcontroller or a single board computer).

Besides the large number of hardware peripherals available, a key feature of this family of microcontrollers is the event system. The event system (EVSYS) enables direct peripheral-to-peripheral signalling. It allows a change in one peripheral (the event generator) to trigger actions in other peripherals (the event users) through event channels, without using the central processing unit (CPU). It is designed to provide short and predictable response times between peripherals, allowing for autonomous peripheral control and interaction, and also for synchronized timing of actions in several peripheral modules. It is thus a powerful tool for reducing the complexity, size, and execution time of the software.

A change of the event generator state is referred to as an event and usually corresponds to one of the peripheral's interrupt conditions. However, compared to software interrupt calls, events can be directly forwarded to other peripherals using the dedicated event routing network. In general, only one event signal can be routed on each channel, but multiple peripherals can use events from the same channel.

The EVSYS can directly connect peripherals such as ADCs, analog comparators, input/output port pins, real-time counter, timer/counters, and the configurable custom logic peripheral.

In order to develop the PKD- and TOT-based acquisition systems, several peripherals have been programmed and routed using the EVSYS, such as the analog comparator acting as a pulse discriminator, some timer/counters, the ADC and more. Extra components interacting with such peripherals have been also added to the design. The specific peripherals, their programming, and reciprocal interaction are going to be described in the next sections.

While similar routing systems are available in other microcontrollers families (such as the more recent AVR128DB, the XMEGA family, PICs, more advanced ARMs, etc.), the choice of the Atmega4809 has been considered a good compromise between performance, cost, the simplicity of AVR low level programming and the large availability of the Arduino programming environment resources and community.
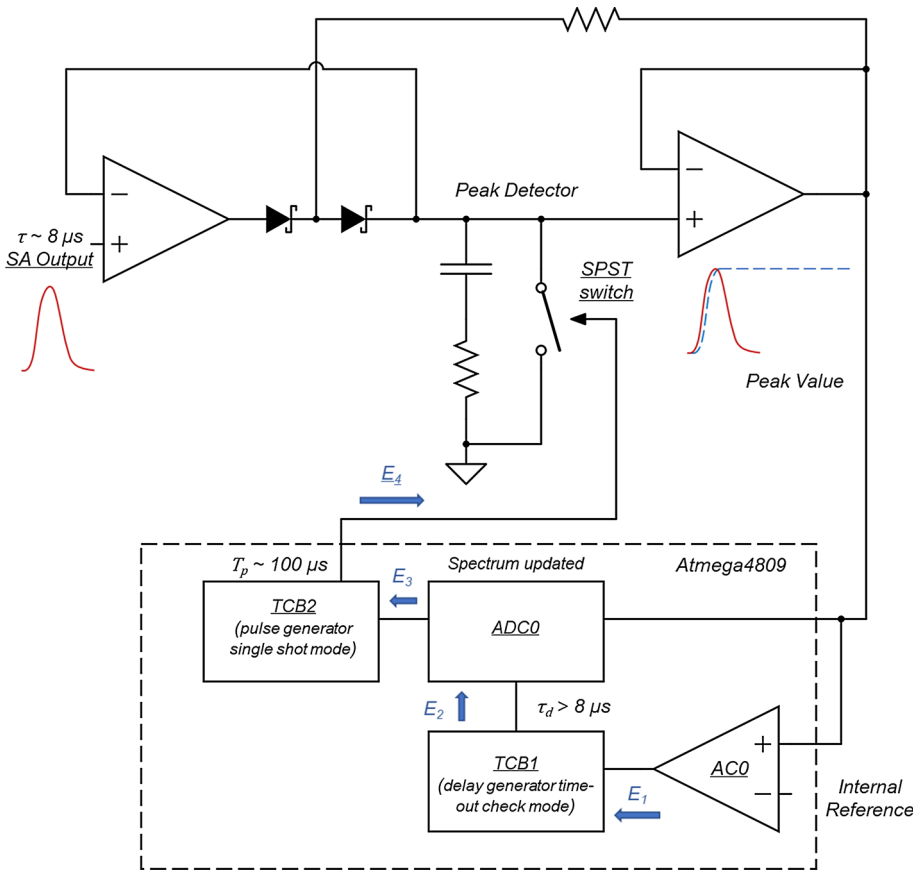
Fig. 4 Peak detection circuit working principle

2.3 Peak detection circuit

Peak detector-based measurements systems are considered the standard approach when an ADC is used to record the height of a current pulse generated inside a detector following ionizing radiation interaction. A peak detector (PKD) is an analog circuit that allows the conversion of transient voltage pulse heights into persistent voltages; it acts as temporary analog memory of the peak value of the pulse. A discriminator is commonly employed to trigger the acquisition through an ADC of the value stored on the PKD, and once the conversion is completed the stored voltage is reset (usually by means of a simple switch).

In our implementation (Fig. 4), the output of the SA is fed into a peak detection circuit employing a high-speed dual-operational amplifier (OPA2365, from TI); the peak value stored on the hold capacitor can be reset through a single pole single throw switch or SPST switch (TMUX1101, from TI). The peak value is compared to an internal voltage reference (scaled by means of an internal digital-to-analog converter) by an analog comparator peripheral integrated in the Atmega4809. When the output of the peak is higher than the threshold, an event (E_1) is generated and routed through the EVSYS to a general purpose 16 bits timer/counter: TCB1. TCB1, configured in time-out check mode, acts as a delay generator.
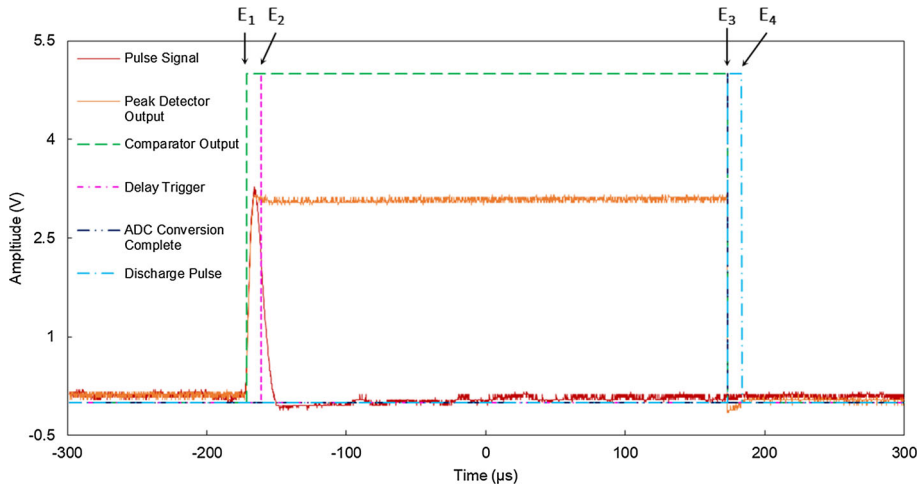
Fig. 5 Pulse, peak detection signals and events concerning the working principle of the PKD circuitry

A delay generator is required to avoid the ADC0 peripheral to trigger a conversion before the peaking value is reached by the peak detection circuit. After a delay time τ_d, a second event (E_2) is generated which triggers the ADC conversion (set to 10 bits resolution or 1024 channels): the new value is then added to the temporary spectrum by the CPU. Upon completion of the ADC conversion, a new event is generated (E_3) which triggers a second timer/counter, TCB2. TCB2, configured in single shot mode, acts as a monostable multi-vibrator generating a digital pulse (having an arbitrary duration T_p longer than the time required to reset the peak detector). The digital pulse triggers the SPST switch through a fourth event (E_4). Since the EVSYS is used to interconnect the peripherals, the behaviour of the circuit is completely predictable, and the CPU is free to manage only the update of the spectrum by adding in the new pulse height value.

The main signals and events of the PKD circuitry operation, acquired with a LeCroy WaveAce 101 digital oscilloscope, are shown in Fig. 5.

2.4 Time over threshold circuit

Time over threshold (TOT) measurement systems have several advantages over conventional measurement systems where analog-to-digital converters (ADCs) are used to collect the height of the pulses [15–17]. Circuit simplicity brings advantages to potentially achieve higher levels of channel density and lower power consumption. However, since the relation between the TOT and the charge deposited in a detector is strongly nonlinear, some digital processing (for example a look-up table) is required to properly estimate the energy released by ionizing radiation in the detector itself. A slightly modified version of TOT, often named "dynamic TOT method" (dTOT), can instead be used to estimate pulse height from the temporal width of a pulse obtained by comparing the input signal to a threshold voltage which changes in a dynamic way. Such method can improve linearity, achieves a wider dynamic range, and also shortens pulse width, which is desirable to reduce the dead time and improve the maximum counting rate.

The dynamic threshold is commonly implemented using a positive feedback from the output of the discriminator to the threshold level itself. A dedicated threshold generating

module is triggered after the input signal comes over an initial threshold level, and the dynamically changing threshold level ramps-up until it crosses the input signal. The time from the initial threshold crossing until the threshold reaches the input signal is the output of the dynamic TOT circuit. A simple timer/counter can be used at this level to perform a time to digital conversion. By choosing the adequate function to generate the variable threshold and by setting specific parameters of the acquisition method, a linear relation between the input charge and TOT can be obtained.

The initial threshold is usually set to a relatively low level (just higher of the baseline noise level), and the first crossing with the input signal can be used to derive the timing information. As shown in [16], maximum linearity is achieved when the shaping time of the SA (τ) matches the time constant of the dynamic threshold positive feedback network (τ').

In our implementation (Fig. 6), the output of the SA is compared to the dynamic threshold by means of the analog comparator peripheral integrated in the Atmega4809. When the output of the SA is higher than the threshold, an event (E_1) is generated and routed through the EVSYS to two general-purpose 16 bit timer/counters: TCB0 and TCB1. TCB0, configured as an input capture unit, performs the measurement of the pulse width which is going to be associated with the height of the pulse and stored inside a 1024 channel temporary spectrum; TCB1, configured in time-out check mode, acts as a delay generator. A delay generator is required to avoid the threshold to cross the pulse signal before reaching its peak. The optimum value for the delay (τ_d) has been shown to be the same as τ and τ'. After τ_d, a second event (E_2) is generated which triggers a third timer/counter: TCB2. TCB2, configured in single shot mode, acts as a monostable multi-vibrator generating a digital pulse (having an arbitrary duration T_p longer than the SA output pulse). The digital pulse triggers a single pole double throw or SPDT switch (TMUX1237, from TI) through a third event (E_3), which allows to generate the dynamic threshold by connecting the feedback network to two alternate, fixed value outputs of an external digital-to-analog converter (MCP4822, from Microchip). Since the EVSYS is used to interconnect the peripherals, the behaviour of the circuit is once again completely predictable, and the CPU is free to manage only the update of the spectrum by adding in the new pulse width value. Moreover, the delay and pulse generators are initialized in software granting a higher degree of customization compared to a completely hardware-based solution.

Prior to the practical implementation, the proposed circuit was simulated using the TINA simulation environment in order to compare the potential linearity improvement between using the standard TOT versus the dynamic TOT approach (Fig. 7). The simulation was performed in response to charge pulses with increasing values (5 to 30 fC) and using the time constants and delays described in this section ($\tau = \tau' = \tau_d = 8\ \mu s$). Different values of the baseline threshold level were also simulated. After assessing the potential improvement of the linearity of the dTOT approach compared to the standard TOT technique, the circuit was designed, realized, assembled and tested.

Since the Atmega4809 uses a 20 MHz clock frequency, all the timers and counters have been set with a time resolution of 50 ns. While considered already appropriate for the task of providing a coarse energy resolution, the time resolution may be increased (by modifying the underlying hardware as well) in order to improve the performance of the gamma spectroscopy and detection system. The main signals and events of the dTOT circuitry operation, acquired with a LeCroy WaveAce 101 digital oscilloscope, are shown in Fig. 8.
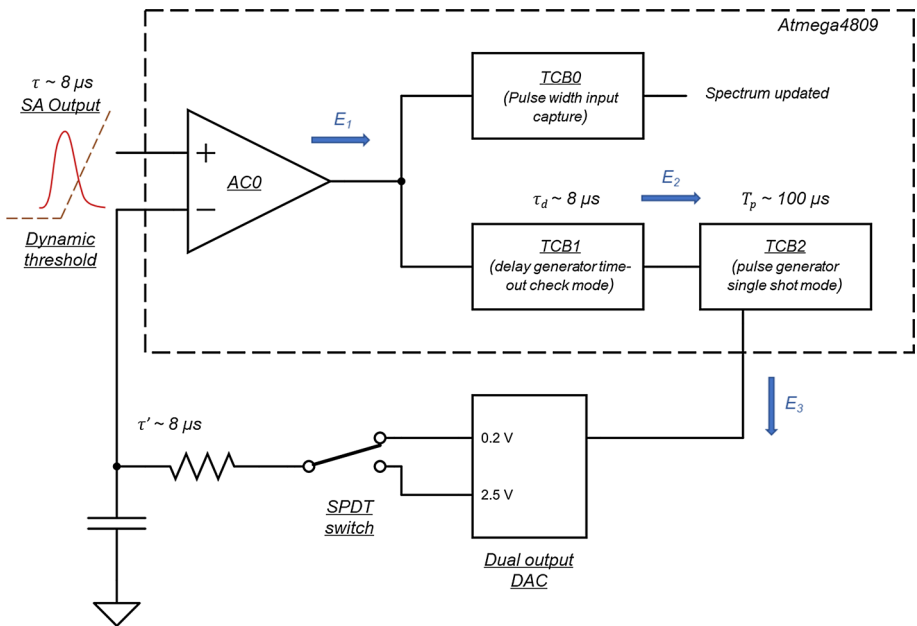
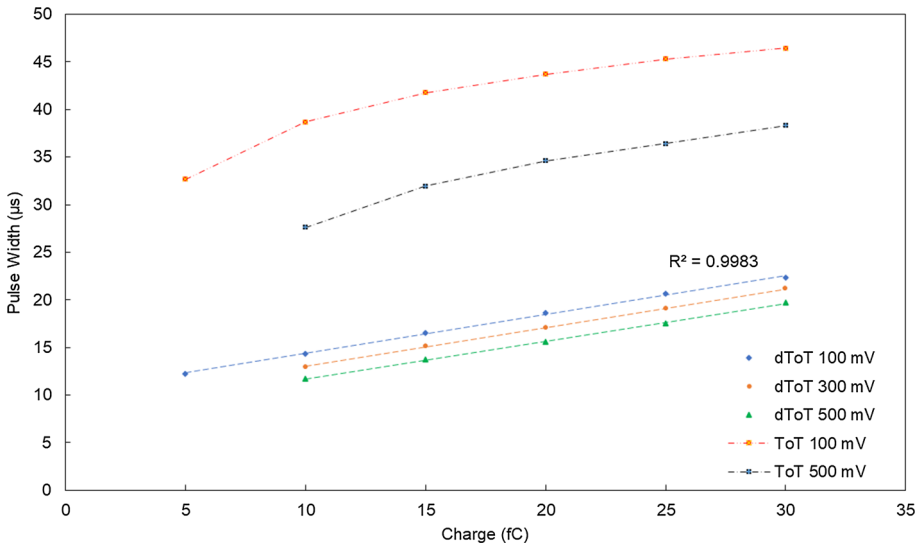**Fig. 6** Dynamic time over threshold circuit working principle

Fig. 7 Comparison in terms of linearity versus charge between the Standard and the dynamic time over threshold approach

2.5 Radio frequency trans-receiver module

The use of a simple radio frequency trans-receiver module (NRF24L01+, Nordic Semiconductor) has also been foreseen in the final design of the apparatus in order to communicate
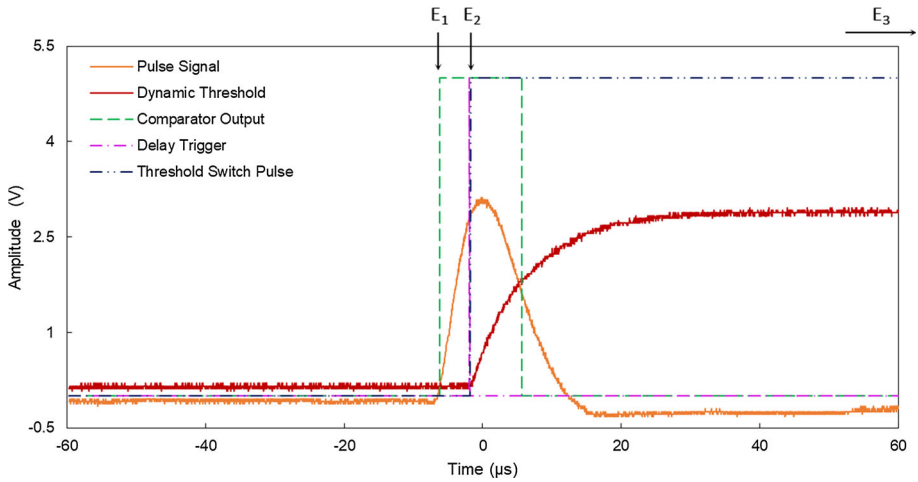
Fig. 8 Pulse, dynamic threshold signals and events concerning the working principle of the dTOT circuitry
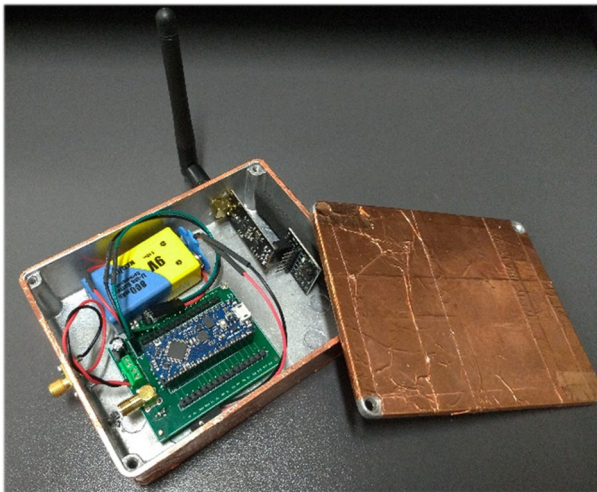
Fig. 9 Data acquisition system and radio frequency trans-receiver module assembly

data with the ground station in real-time. Two identical modules are required: the first one, acting as a transmitter, must be interconnected with the data acquisition system and mounted on the airborne drone unit; the second one, acting as a receiver, must be installed into a gateway (for example another development board of the same kind) to communicate with the ground station. The key features of the module are the worldwide 2.4 GHz ISM band operation and the capability of transmitting data up to 2 Mbps on air data rates up to a distance of 1100 m. The enclosure containing the data acquisition system and the trans-receiver is shown in Fig. 9.

3 Results

To establish our system's charge linearity, calibration and electronic noise, a lab-made saw-tooth waveform generator (built upon a digital-to-analog converter integrated in an Atmel SAM3×8e Microcontroller) was used to inject a known charge into a testing capacitor connected to the input of the CSP. The rise time of a single voltage step was roughly equal to 20 ns, while the negative ramp duration was set to 4 ms, de facto achieving a wave frequency of roughly 250 Hz. The nominal capacitance value used to inject the charge was 2.2 pF (± 10%). In order to further scale down the injected charge (given the high sensitivity of the CSP chosen), a resistor divider having a nominal attenuation equal to 0.01 was also used. The nominal value of the injected charge was then given by:

$$Q = 0.01 \times V_{\text{step}} \times C_{\text{test}} \tag{1}$$

The AFE was enclosed in an aluminium box (1 mm thick wall) and wrapped in a conductive copper tape (100 μm thick) in order to shield the sensitive stages of the front-end from environmental electro-magnetic interference (EMI). The data acquisition systems were placed inside a separate box: the output signal from the shaping amplifier was fed to next stages using SMA cables and connectors assemblies.

By choosing the sawtooth amplitude accordingly, the charges injected were nominally set to 1.2, 2.4, 3.5, 4.7, and 5.9 fC. The value of the maximum injected charge was chosen by observing that the peak value of the pulses in response to an exposure with a ^{60}Co RN source was roughly equal to the response obtained using such charge.

The output signal from the shaping amplifier was also split and fed to a channel of a LeCroy WaveAce 101 digital oscilloscope to check the behaviour of the front-end and the baseline noise level. The baseline noise level, in absence of the PIN diode and measured directly from the output of the shaping amplifier, was found to be in the order of 50 mV$_{\text{pp}}$. Since an amplification stage providing a non-inverting gain equal to three was present on board before the conversion for both data acquisition systems, such level of noise was expected to be three times higher at the end of the amplification chain. Therefore, the baseline voltage threshold level for the discriminator in both systems was set to 200 mV in order to avoid unwanted counts triggered from pure electronic noise.

3.1 Peak detection (PKD) linearity and electronic noise

Results of the charge calibration for the PKD system are shown in Figs. 10 and 11. From the histogram of the values obtained from the ADC, the level of noise associated with the data acquisition chain can be immediately assessed. Moreover, the step result is satisfactorily fit to a linear function, and the charge resolution (expressed as % FWHM) is in the order of magnitude of the uncertainty which can be expected when the system will be interfaced with a Cs(Tl) scintillation detector [9].

We can conclude that the system can definitely be used to acquire the signals produced by the AFE, and by accepting the necessity to implement a peak detection circuit for each channel, it is a promising solution to perform basic gamma detection and spectroscopy tasks.

3.2 Dynamic time over threshold (dTOT) linearity and electronic noise

Results of the charge calibration for the TOT and dTOT systems are shown in Figs. 12 and 13. It is clear that the normal TOT conversion technique (without the dynamic threshold) suffers from very poor linearity and a high level of noise. The loss of FWHM in the charge resolution is
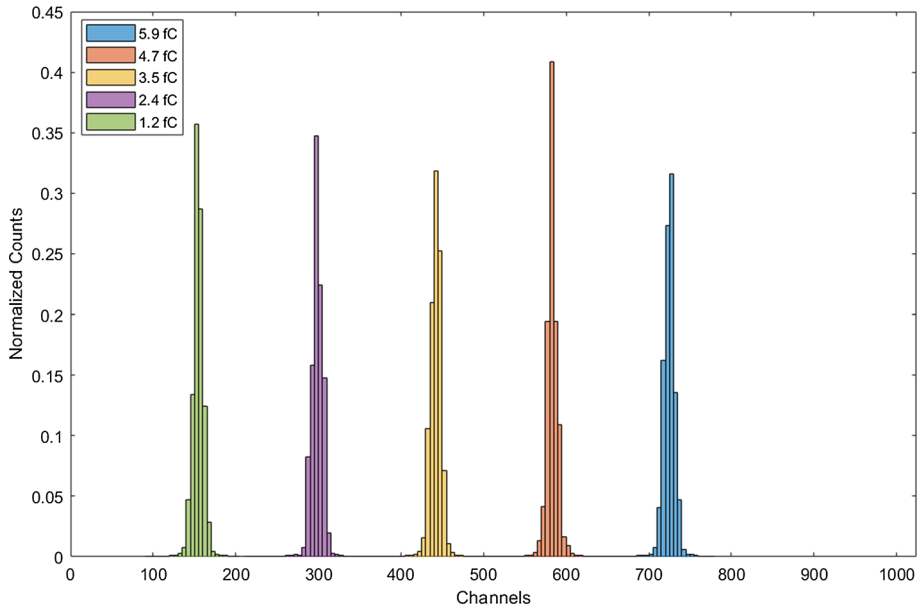
Fig. 10 Histogram (normalized counts) of the values obtained from the ADC conversion in response to known injected charges
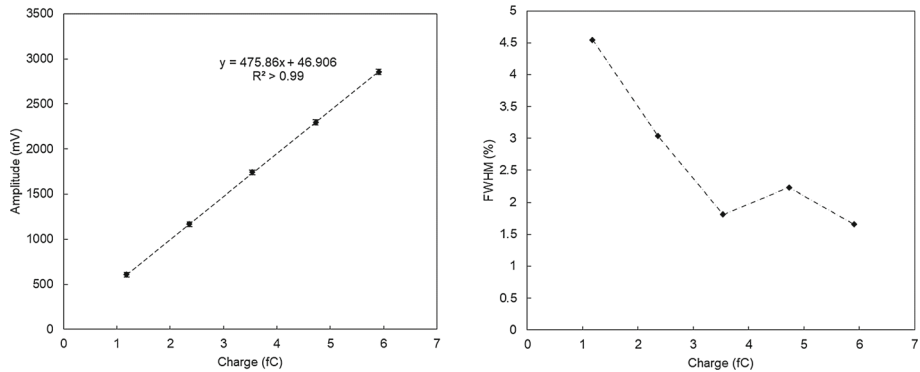

Fig. 11 Linear fit of the PKD response to known injected charge (left) and charge resolution expressed as FWHM (right)

mainly due to the effect of jitter when the pulse signal approaches back the baseline threshold level: since the tail of the pulse signal is relatively slow, a small level of noise is traduced in a large variation of the timestamp associated with the crossing point between the signal and the threshold. This effect is clearly mitigated by the dynamic threshold, since the signal crosses back the threshold with a sharp edge thus decreasing the effect of jitter. The linearity of dTOT results also improved compared to TOT, and it is almost comparable with the value obtained using the PKD technique. The dynamic range still results slightly compressed, but the FWHM in dTOT is almost the same (if not lower) compared to the PKD system.

While the use of normal TOT is discouraged because of bad linearity and high noise sensitivity, both PDK and dTOT techniques are promising to design compact, low power and
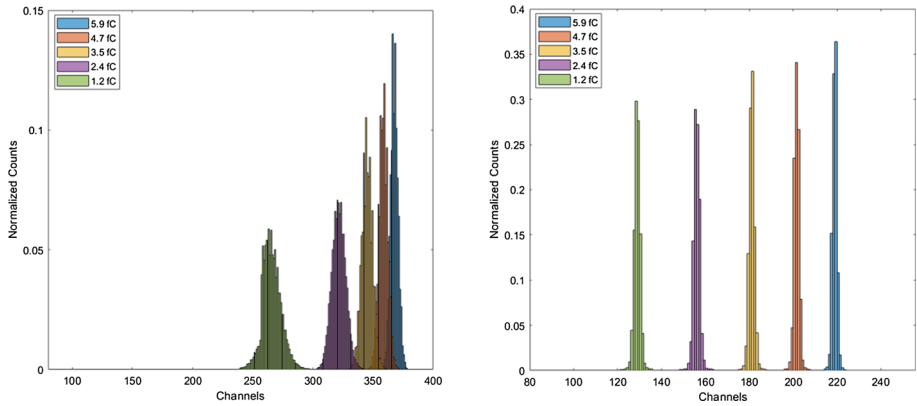
Fig. 12 Histogram (normalized counts) of the values obtained from normal TOT conversion (left) and dynamic TOT (right) in response to known injected charges
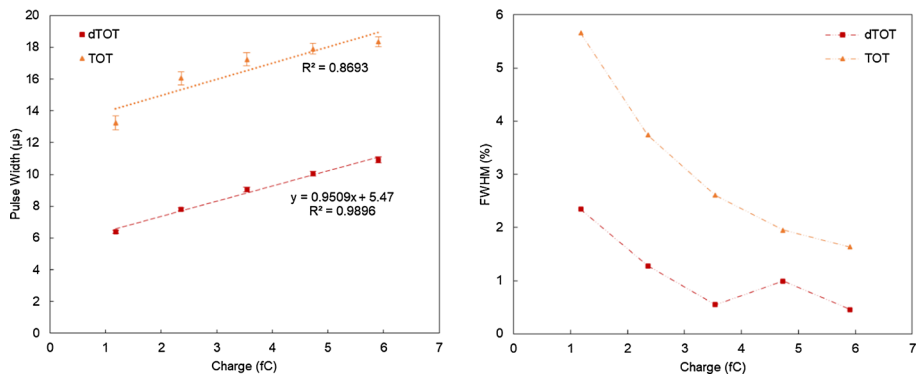

Fig. 13 Linear fit of the TOT vs dTOT response to known injected charge (left) and charge resolution expressed as FWHM (right)

lightweight gamma detection and spectroscopy systems to be mounted on airborne drone units.

3.3 Response to RN sources

The response of the detection systems has been tested by exposing the prototypes to ^{137}Cs and ^{60}Co radioactive sources. The tests have been conducted to assess in a qualitative way the goodness of the conversion methods chosen to digitize and collect the pulse signals from the scintillation detector in terms of their capability to represent the spectral features typical of gamma scintillation spectroscopy of the chosen emitters, such as gamma photopeaks, and compton valley, edge, continuum.

As shown in Figs. 14 and 15, the gamma photopeaks for ^{137}Cs (662 keV) and ^{60}Co (1.17 and 1.33 meV) are clearly visible for both conversion techniques. The typical features of the spectra, such as the Compton valleys, edges and continuum, are present as well. A certain level of noise can also be observed, and it will need to be worked out by decreasing the electronic noise associated with the acquisition chain and by optimizing the elements of design of the detector.
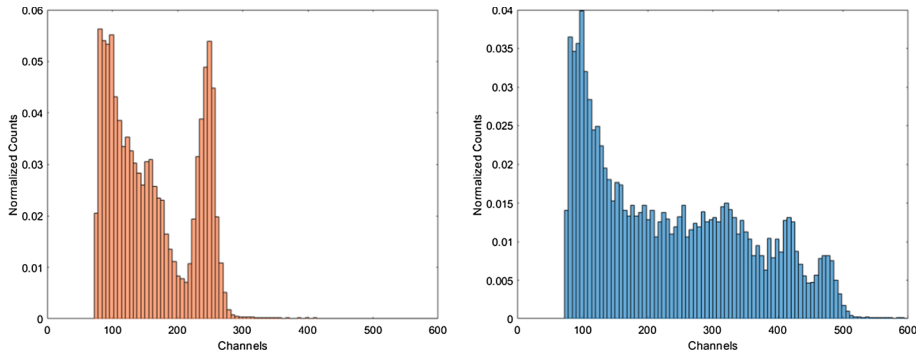
Fig. 14 ^{137}Cs (left) and ^{60}Co (right) spectra acquired using the conversion system based on a PKD approach
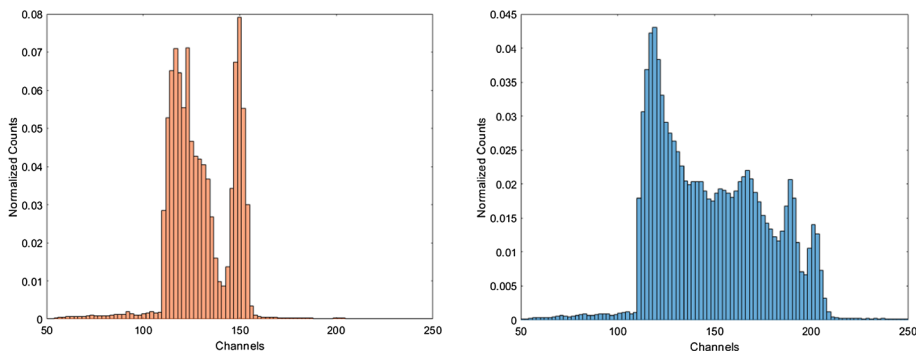

Fig. 15 ^{137}Cs (left) and ^{60}Co (right) spectra acquired using the conversion system based on a dTOT approach

4 Future developments

We have shown the fundamental methods of charge calibration and spectrum measurement for both PDK and dTOT systems. Such experiments represent the required steps towards demonstrating sufficient linearity and noise levels for gamma ray spectroscopy. Energy calibration, energy-dependent resolution, efficiency calibration and limits of detection are obvious next steps.

Studies involving a comparison and design aspects of different detectors and their sensitivity to environmental parameters (such as temperature or humidity) should also be carried out.

However, it is of our interest to offer the reader also an overview of the mid to long-term steps of the work which are necessary to effectively use the designed gamma detection and spectroscopy systems on an UAV to carry out radiation monitoring tasks.

Commonly, the gamma radiation detector together with the AFE are addressed as the front-end, while the block consisting in the data acquisition system, and the main processing algorithms are identified as the back-end. This work focussed mainly on the development and characterization of the front-end and data acquisition part of the back-end block (Fig. 16).

The raw gamma radiation data need to be processed not only to complete the characterization of the front-end and data acquisition system, as previously stated, but also to allow the UAV (equipped with the detection system) to carry out specific radiation monitoring tasks, such as local radiation contamination mapping, source localization and plume-tracking in
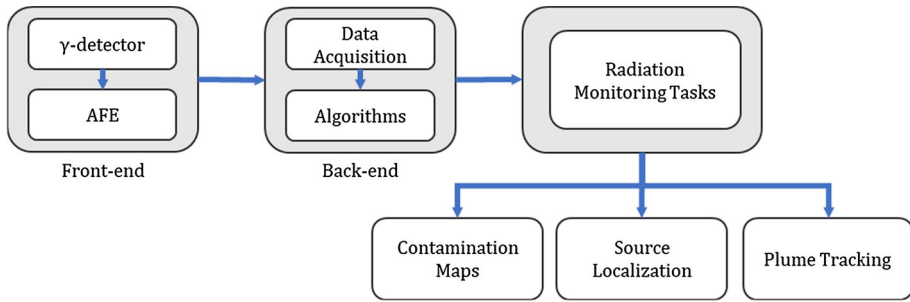
Fig. 16 Overview of the development of gamma radiation detection and spectroscopy system able to carry out radiation monitoring tasks

case of diffused contamination. The algorithms necessary to perform such tasks will require once again a multiple-step approach, starting from true count and spectroscopy processing of the gamma radiation data [9, 19–22] and moving towards the application of statistical and machine learning methods to allow the drone to track the radioactive plume and to identify potential RN sources dispersed in an area of interest [23–25].

The final goal is to develop an UAV able to carry out all the previously mentioned tasks in an autonomous way with reasonable accuracy in order to become a handy tool to assess the risk for first responders or military personnel who may be exposed to an unacceptable amount of radiation during their intervention, while keeping the development and maintenance costs low.

5 Conclusions

In this work, a compact, low-power, low-weight and affordable gamma ray detection and spectroscopy system was designed, realized and tested. The system is meant to be mounted on a mini-multirotor UAV (MTOW less than 25 kg) to reduce first responders' exposure, casualties and waste of time during RN emergencies.

The designed system is based on a commercial analog front-end (AFE) consisting in a charge sensitive preamplifier (CSP) and a shaping amplifier (SA) interfaced with an Atmega4809 microcontroller (MCU). The MCU, together with some extra components and integrated circuits, was configured to fulfil the role of a multi-channel analyzer (MCA) using both peak detection (PKD) and dynamic time over threshold (dTOT) conversion techniques.

A radio frequency trans-receiver communication module was also installed on the platform to guarantee a medium-long distance communication range capability.

The working principles and basic components required to realize the platform were reviewed first, then the attention was focused on the specific system's individual components and on some of the underlying physics. Moreover, the actual realization and testing procedures of the prototypes were described and presented together with the results of a charge calibration. The experiments demonstrated an adequate linearity and noise levels for gamma ray spectroscopy in both PKD and dTOT approaches.

Finally, gamma ray spectra were acquired by exposing the systems to sealed RN sources, and a list of the next steps required to complete the characterization of the platform was introduced.

The future developments of this project consist in completing the characterization of the platform, implementing dedicated algorithms and mounting the detection system on an UAV having the goal of carrying out specific radiation monitoring tasks with reasonable accuracy in order to become a tool to assess the risk for first responders who may become exposed to an undesirable amount of radiation during intervention, while keeping the development and maintenance at low costs.

Data Availability Statement Open source. Libraries, whether if necessary, are released under MIT, Apache and BSD license.

Author contributions AC helped in conceptualization, formal analysis, investigation, experimental activities, methodology and writing—original draft; FF and PG were involved in funding acquisition; PG, DDG, AM and FDE contributed to project management; PG, DDG, AM and FDE contributed to supervision; AM, DDG, FF, LM, PG and FDE were involved in writing—review and editing. All authors have read and agreed to the published version of the manuscript.

Compliance with ethical standards

Conflict of interest The authors declare no conflict of interest.

References

1. Y. Cao, X.-B. Tang, P. Wang, J. Meng, X. Huang, L.-S. Wen, D. Chen, Spectrum correction algorithm for detectors in airborne radioactivity monitoring equipment NH-UAV based on a ratio processing method. Nucl. Instrum. Methods Phys. Res. Sect. A **797**, 290–296 (2015)
2. J. MacFarlane, O. Payton, A. Keatley, G. Scott, H. Pullin, R. Crane, M. Smilion, I. Popescu, V. Curlea, T. Scott, Lightweight aerial vehicles for monitoring, assessment and mapping of radiation anomalies. J. Environ. Radioact. **136**, 127–130 (2014)
3. Y. Sanada, T. Torii, Aerial radiation monitoring around the Fukushima Dai-Ichi nuclear power plant using an unmanned helicopter. J. Environ. Radioact. **139**, 294–299 (2015)
4. J. Towler, B. Krawiec, K. Kochersberger, radiation mapping in post-disaster environments using an autonomous helicopter. Sensors **4**, 1995–2015 (2012)

5. K. Kurvinen, P. Smolander, R. Pöllänen, S. Kuukankorpi, M. Kettunen, J. Lyytinen, Design of a radiation surveillance unit for an unmanned aerial vehicle. J. Environ. Radioact. **81**(1), 1–10 (2005)

6. NATO. [Online]. Available: http://nso.nato.int/nso/zPublic/stanags/CURRENT/4586EFed04.pdf

7. NATO, *ADatP-36 STANAG 5527 Friendly Force Tracking Systems (FFTS) Interoperability* [Online]

8. NATO, *APP-11 STANAG 7129 Nato Message Catalogue* [Online]

9. G.F. Knoll, *Radiation Detection and Measurement* (Wiley, 2010).

10. G. Gilmore, *Practical Gamma-Ray Spectroscopy* (Wiley, 2008).

11. M. Grodzicka-Kobylka, M. Moszyński, T. Szczęśniak, Silicon photomultipliers in gamma spectroscopy with scintillators. Nucl. Instrum. Methods Phys. Res. Sect. A **926**, 129–147 (2019)

12. D. Cester, M. Lunardon, G. Nebbia, L. Stevanato, G. Viesti, S. Petrucci, C. Tintori, Pulse shape discrimination with fast digitizers. Nucl. Instrum. Methods Phys. Res. Sect. A **748**, 33–38 (2014)

13. Microchip Technology, [Online]. Available: https://ww1.microchip.com/downloads/en/DeviceDoc/Atmel-7810-Automotive-Microcontrollers-ATmega328P_Datasheet.pdf

14. Microchip Technology, [Online]. Available: http://ww1.microchip.com/downloads/en/DeviceDoc/ATmega4808-4809-Data-Sheet-DS40002173A.pdf

15. K. Shimazoe, Dynamic time over threshold method. EEE Trans. Nucl. Sci. **59**(6), 3213–3217 (2012)

16. T. Orita, K. Shimazoe, and H. Takahashi, Dynamic time-over-threshold method for multi-channel APD based gamma-ray detectors, in *IEEE Nuclear Science Symposium and Medical Imaging Conference Record (NSS/MIC),* pp. 824–826 (2012)

17. R. Liu, M. Zeng, Y. Tian, Y. Yang and X. Wang, "Application of the dynamic time over threshold method for semi-Gaussian signals," *Journal of Instrumentation,* vol. 13, no. 02, 2018.

18. P. Lecoq, A. Gektin, M. Korzhik, *Inorganic Scintillators for Detector Systems* (Springer, 2017).

19. K. Bargholz, U. Korsbech, Conversion of airborne gamma ray spectra to ground level air kerma rates. Radiat. Prot. Dosimetry. **73**(1–4), 127–130 (1997)

20. M. Albéri, M. Baldoncini, C. Bottardi, E. Chiarelli, G. Fiorentini, K. Raptis, E. Realini, M. Reguzzoni, L. Rossi, D. Sampietro, V. Strati, F. Mantovani, Accuracy of flight altitude measured with low-cost GNSS, radar and barometer sensors: implications for airborne radiometric surveys. Sensors **17**(8), 1889 (2017)

21. E. Druker, Airborne gamma-ray spectra processing: extracting photopeaks. J. Environ. Radioact. **187**, 22–31 (2018)

22. G. Popescu, S. Herman, S. Glover, Compton background suppression with a multi-element scintillation detector using high speed data acquisition and digital signal processing. J. Radioanal. Nucl. Chem. **307**, 1949–1955 (2016)

23. M. Alamaniotis, J. Mattingly, L.H. Tsoukalas, Kernel-based machine learning for background estimation of NaI low-count gamma-ray spectra. EEE Trans. Nucl. Sci. **60**(3), 2209–2221 (2013)

24. L. Ruirui, H. Kathryn, L. Xinzhi, Discussion on one algorithm for mapping the radiation distribution on contaminated ground. Health Phys. **109**(1), 25–34 (2015)

25. M. Silic, K. Mohseni, Field deployment of a plume monitoring UAV flock. IEEE Robot. Autom. Lett. **4**(2), 769–775 (2019)